ELSEVIER

Earth and Planetary Science Letters 203 (2002) 817–828

EPSL

www.elsevier.com/locate/epsl

Polytypism and microstructures of the mixed-layer member B_2S, $CaCe_3(CO_3)_4F_3$ in the bastnaesite-(Ce)–synchysite-(Ce) series

Dawei Meng [a,*], Xiuling Wu [a], Yujing Han [a], Xin Meng [b]

[a] *Testing Center, China University of Geosciences, Wuhan 430074, PR China*
[b] *Faculty of Foreign Language, Wuhan University, Wuhan 430070, PR China*

Received 5 April 2002; received in revised form 29 August 2002; accepted 30 August 2002

Abstract

The crystal structures and polytypism of bastnaesite-(Ce) ($CeCO_3F$, B layer) and synchysite-(Ce) ($CeCO_3F{\cdot}CaCO_3$, S layer) mineral series are very complicated in Sichuan Province, Southwest China. Four new polytypes: 6*R*, $2H_2$, 4*H* and 12*H* of the mixed-layer member $CaCe_3(CO_3)_4F_3$ (B_2S) of this series were discovered by X-ray diffraction analyses and high resolution transmission electron microscopy, structural symmetry, cell and subcell parameters, possible space group, and structural stacking mode (*dededgfgl*...). They reveal that the mixed-layer member B_2S is formed by the ordered stacking of two structural unit layers of bastnaesite-(Ce) (B layer) and one unit layer of synchysite-(Ce) (S layer) along the *c* direction. The forming of the new polytypes may depend on distributions and the periodical variation of orientation of the $[CO_3]$ groups between the unit layers of B_2S. We have observed the {0001} microtwin of the 6*R* polytype and the syntactic intergrowths among the different polytypes formed by stacking faults in B_2S.

Keywords: bastnaesite–synchysite; polytype; mixed-layer; X-ray diffraction analysis; HRTEM; transmission electron microscopy

1. Introduction

Bastnaesite-(Ce), $Ce(CO_3)F$ and synchysite-(Ce), $CaCe(CO_3)_2F$ are the two end-members of the calcium rare-earth (Ca-RE) fluorocarbonate mineral series, constituting B layers and S layers of this polytypic mineral group. Donnay et al. [1] originally proposed that other minerals of this series can be characterized in terms of these two end-members, for example parisite-(Ce) $[CaCe_2(CO_3)_3F_2]$ as BS and roentgenite-(Ce) $[Ca_2Ce_3(CO_3)_5F_3]$ as BS_2 [1,2]. Minerals of this series are often affected by stacking faults, disorder of chemical composition, superstructures, twinning, polytypism and syntactic intergrowths during the course of crystallization and crystal growth along with other mineral phases, making it difficult to obtain crystallographic data on the fine structures of the minerals. Van Landuyt et al. discovered three new mixed-layer compounds (B_3S_2, B_3S_4 and BS_4) by transmission electron mi-

* Corresponding author. Tel.: +86-27-87482596; Fax: +86-27-87801763.
E-mail addresses: dwmeng@cug.edu.cn (D. Meng), dwmeng@cug.edu.cn (X. Wu), zuoxzeng@public.wh.hb.cn (Y. Han), dwmeng@cug.edu.cn (X. Meng).

0012-821X/02/$ – see front matter
PII: S0012-821X(02)00947-0

croscopy (TEM) [3]. Later investigations have found 23 more B_mS_n new mixed-layer members [4–7] and 17 new polytypes of both parisite-(Ce) [8–10] and B_mS_n new mixed-layer members [5,11,12].

The microstructures of members of the Ca-RE fluorocarbonate mineral series occurring within an alkali aegirine granite massif in Sichuan Province, Southwest China, have been studied in detail by single-crystal X-ray diffraction (XRD) analysis. Areas were selected to obtain electron diffraction (SAED) and high resolution transmission electron microscope (HRTEM) data, revealing four new polytypes of mixed-layer member $CaCe_3(CO_3)_4F_3$ (B_2S) and also confirming three polytypes ($2H_1$, $12R$ and $24R$) of B_2S found by Wu et al. using the crystal lattice imaging technique [4,11,12]. The investigation of the crystallographic system, cell parameters, chemical formula, space group, structural stacking mode and microtwin as well as syntactic intergrowth between polytypes of B_2S is described.

2. Samples and experimental technique

The samples for this investigation were crystal grains of Ca-RE fluorocarbonate minerals (0.08–0.3 mm in diameter) from a rare-earth mineral deposit within the Sichuan alkali aegirine granite massif. 'Polycrystals' with syntactic intergrowths were selected for TEM analysis after single-crystal XRD analyses, crushed into fine fragments and suspended in absolute alcohol. A drop of the suspension was put on a copper grid coated with a perforated carbon film, in turn coated with gold. It was examined at 200 kV using a JEOL-2000EX II HRTEM equipped with a top-entry goniometer stage ($\pm 10°$ tilt) and an ultra-high-resolution pole piece (Cs = 0.7 mm) with an interpretable point resolution of 0.21 nm. SAED patterns at 120 kV on a Philips-CM 12 ($\pm 45°$ tilt, Cs = 2.0 mm) TEM.

The single crystals of a mixed-layer member (B_2S) discovered by XRD analysis are columnar, 0.1–0.3 mm in diameter with transverse striations on the crystal surface (Fig. 1). They are yellow or off-white in color, transparent, with glassy or greasy luster and few cleavages, similar optical properties to those of parisite-(Ce) [13]. X-ray single-crystal diffraction analyses were performed by using an RU-200B single-crystal diffractometer with rotation angles of 30–60° with CuKα radiation ($\lambda = 0.15418$ nm) and no filter at 40 kV, 100 mA and 2–4 h exposure.

2.1. X-ray single-crystal diffraction studies

Rotation diffraction patterns of the mixed-layer member (B_2S) about the c axis of single crystals (Fig. 2) were observed in X-ray single-crystal diffraction studies. Local enlarged patterns (Fig. 3) were obtained from the diffraction spot array between 11 $\bar{2}0$ and 11 $\bar{2}L_1'''$ in the rotation diffraction pattern around the c axis of Ca-RE fluorocarbonate minerals (B, B_2S, BS, BS_2 and S). Donnay et al. [1] have previously described the B, BS, BS_2 and S XRD patterns. In Figs. 2 and 3 crucial differences in diffraction intensity, repeat period and distributional positions of diffraction spots in the spot array (except for the strongest array 11 $\bar{2}0$, 11 $\bar{2}L_1'''$, 11 $\bar{2}L_2'''$, ...) can be seen between the mixed-layer member (B_2S) and the other known Ca-RE fluorocarbonate minerals [1,13]. They can be summarized as follows:

1. In the rotation diffraction pattern (Fig. 2) about the c axis, the diffraction spot array $H-K = 3n$ ($n = 0, 1, 2,...$) and the strongest spots 11 $\bar{2}L_i'''$ ($i = 0, \pm 1, \pm 2,...$) reveal the existence of pseudo-periods a' and c''' ($c''' = 0.473$ nm).
2. The distribution between strong diffraction spots and weak ones is similar to that of parisite-(Ce) and synchysite-(Ce), but the distributional positions and repeat period of the diffraction spots are different. There are three stronger diffraction spots between the strongest ones, 11 $\bar{2}0$ and 11 $\bar{2}L_1'''$, revealing a subperiod c'' ($c'' = 4c''' = 1.892$ nm).
3. In the spot array $H-K = 3n$ between the strongest and stronger spots, every four weak spots representing the subperiod c' ($c' = 2c'' = 8c''' = 3.785$ nm) are distributed alternately with three stronger ones. Very weak diffraction spots $H-K \neq 3n$ are scattered at 1/3 or 2/3 the distance between two adjacent arrays close to the

zero array, so the superstructural period is $c = 3c' = 6c'' = 24c''' = 11.354$ nm. Thus the new polytype (6*R*) of B_2S is rhombohedral (Table 1).

4. By using the Donnay et al. [1] plot of the pseudo-period c''' obtained by X-ray single-crystal diffraction analysis against composition in mol% $CaCO_3$, the proportion of $CaCO_3$ can be inferred. $c''' = 0.473$ nm, giving 25 mol% $CaCO_3$, i.e. $Ce(CO_3)F:CaCO_3 = 3:1$. The chemical formula of this mixed-layer member (B_2S) is therefore $CaCe_3(CO_3)_4F_3$, composed of two formula units of bastnaesite-(Ce) ($2Ce(CO_3)F$) and one of synchysite-(Ce) ($CaCe(CO_3)_2F$). It represents a mixed-layer member BBS = B_2S intermediate between bastnaesite-(Ce) and parisite-(Ce).

2.2. HRTEM observations and discussion

The HRTEM specimens were carefully selected after X-ray single-crystal diffraction analysis. The crystal appearance and other characteristics are similar to those of parisite-(Ce), but in fact most of the specimens were 'polycrystals', composed of interlayers of bastnaesite-(Ce) [B layer, CeF-CO_3], parisite-(Ce) (BS layer), roentgenite-(Ce) (BS_2 layer) and synchysite-(Ce) [S layer, CeF-CO_3-Ca-CO_3]. The crystal structures characteristic of the Ca-RE fluorocarbonate minerals are rhombic planes constituted of heavy atoms of Ce and Ca distributed alternately normal to the trigonal or hexagonal axis, and triangular planes formed by CO_3 lying parallel to the *c* axis between the CeF and CeF layers, or oblique from the *c* axis between the CeF and Ca layers. Donnay et al. [1] made qualitative descriptions of this mineral using four different layers parallel to the (0001) plane. The four layers are: *d*, CeF ionic layers; *f*, Ca ionic layers: *e*, layers of CO_3 groups between CeF layers, and *g*, layers of CO_3 groups between Ca layer and CeF layer. For example, the stacking layers of bastnaesite-(Ce) (B), parisite-(Ce) (BS), roentgenite-(Ce) (BS_2) and synchysite-(Ce) (S) can be described as *de* (B), *dedgfg* (BS), *dedgfgdgfg* (BS_2) and *dgfg* (S).

2.3. The 6R polytype of B_2S and its microtwin

A set of SAED patterns (Fig. 4a–c) were found around the 000*l* spot array where the crystal zones are [11 $\bar{2}$0] (Fig. 4a), [01 $\bar{1}$0] (Fig. 4b) and [$\bar{1}$2 $\bar{1}$0] (Fig. 4c) respectively, and the angles between two adjacent electron diffraction patterns are 29.9° (between Fig. 4a and b) and 30.2° (between Fig. 4b and c). A reciprocal lattice plane (Fig. 4d) normal to the crystal zone [0001] was constituted according to the three SAED patterns and the

Table 1
Crystal structures of Ca-RE fluorocarbonate mineral series

Name	Space group	Cell				Structural layer stacking mode	Height of layer	Chemical formula	$CaCO_3$	References
		a (nm)	*b* (nm)	*c* (nm)	*β* (°)		(nm)		(mol%)	
Bastnaesite-(Ce)	*P* $\bar{6}$ *2c*	0.716	0.716	0.978	120.00	*de*/...	0.489	$CeCO_3F$	0.00	[1,3,4,14]
B_2S(12*R*)	*R*32 or *R*3*m* or *R* $\bar{3}$*m*	0.711	0.711	22.608	120.00	*dededgfg*/...	1.892	$CaCe_3(CO_3)_4F_3$	25.00	[4,11,12]
Parisite-(Ce)	C2/c or Cc	1.231	0.711	2.825	98.26	*dedgfg*/...	1.413	$CaCe_2(CO_3)_3F_2$	33.00	[8]
Parisite-(Ce)	*R*3 or *R* $\bar{3}$	0.717	0.717	8.478	120.00	*dedgfg*/...	1.413	$CaCe_2(CO_3)_3F_2$	33.00	[1,3,4,9–12,16]
Roentgenite-(Ce)	*R*3 or *R* $\bar{3}$	0.713	0.713	6.940	120.00	*dedgfgdgfg*/...	2.313	$Ca_2Ce_3(CO_3)_5F_3$	40.00	[1–3]
Synchysite-(Ce)	*C*2/*c*	1.233	0.711	1.874	102.68	*dgfg*/...	0.937	$CaCe(CO_3)_2F$	50.00	[1,15]

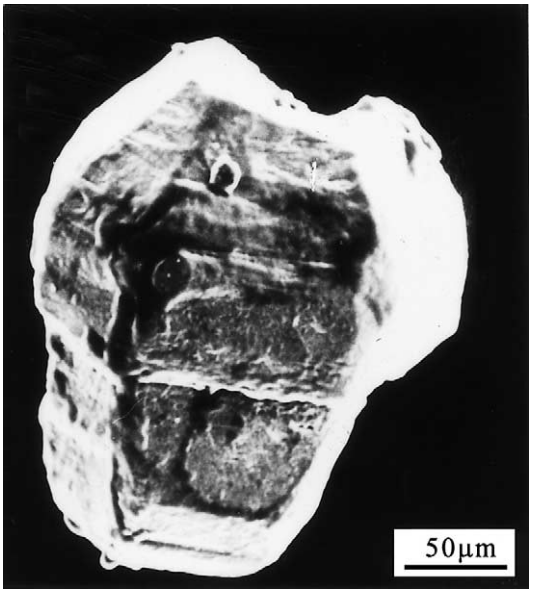

Fig. 1. Scanning electron micrograph of a single crystal of B_2S.

angles between two adjacent zones. In Fig. 4a–c, the diffraction spots produced by this mixed-layer member (B_2S) can be classified into strong, stronger and weak ones. The diffraction spots of the zones [$\bar{1}2\ \bar{1}0$] and [$11\ \bar{2}0$] are characteristic of a distribution in layers parallel to the c direction. The $3n$ ($n=0,\ \pm1,\ \pm2$,...) layers are constituted by strong 00$\underline{24}$ (c'''^*) and stronger diffraction spots have the same arrangement, reflecting the hexagonal subcell $a'c'''$ and $a'c''$ ($c''=4c'''$). The $3n\pm1$ layers constituted by weak spots whose distributional density is twice that in the $3n$ layers, reveal the substructure $a'c'$ ($c'=2c''$) and the superstructure ac ($a=\sqrt{3}a'$, $c=3c'$). There are five extinction spots between 0000 and 0006, the above diffraction spots display rhombohedral (R) lattice symmetry and the reflection condition is $h-k+l=3n$ (Fig. 4a–e and Table 2), so the first strong diffraction spot should be indexed as 00$\underline{24}$ (c'''^*) and the diffraction spot nearest to the transmission spot 0000 should be indexed as 0006 (c''^*) along the c direction. The cell parameters obtained by SAED analysis are $a'=0.412$ nm, $a=0.713$ nm, $c'''=0.471$ nm, $c=3c'=6c''=24c'''=11.304$ nm. The possible space group is $R3$ or $R\bar{3}$. The HRTEM image (Fig. 4e) of the crystal zone [$\bar{1}2\ \bar{1}0$] reveals that the period distance of the structural unit layers CeF-CO_3-CeF-CO_3-CeF-CO_3-Ca-CO_3 is 1.884 nm. The unit layer is formed by the basic layer CeF-CO_3-CeF-CO_3-CeF (*deded*), which is composed of three black streaks (CeF layer), two white thin streaks CO_3 between the black ones and a white thick streak CO_3-Ca-CO_3 (*gfg*). The corresponding stacking mode is *dededgfg*/.... From the chemical composition [$CaCe_3(CO_3)_4F_3$] and the stacking mode, the mixed-layer member can be considered as BBS, i.e. B_2S ($6R$). The projective

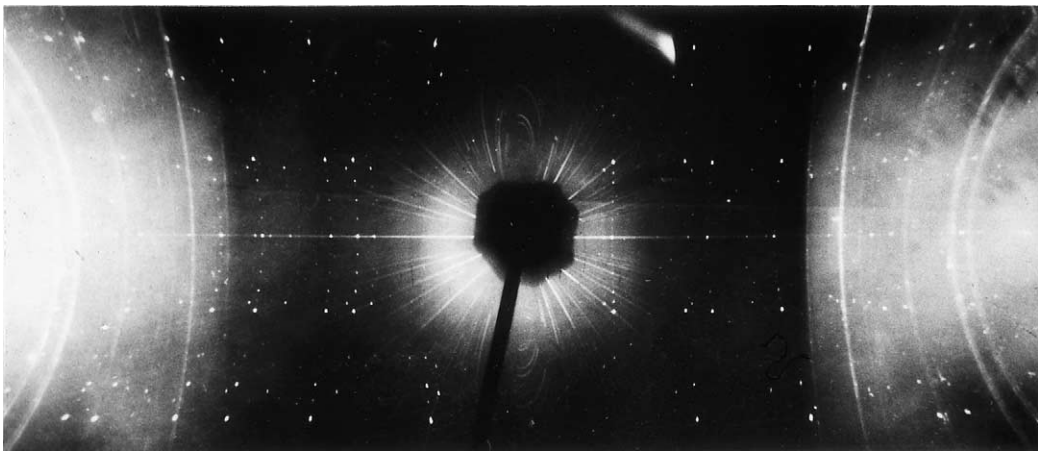

Fig. 2. Single crystal XRD photograph (rotation about the c axis) of the mixed-layer member B_2S (CuKα radiation; 2 h exposure).

Table 2
TEM analyses of seven polytypes of the mixed-layer member B_2S

Polytype	Cell and subcell (nm)				Number of unit layers (*dededgfg*)	Reflection conditions				Possible space group
	a'	a	c'	c		$hkil$	$h\,\bar{h}0l$	$hh2\,\bar{h}l$	0001	
$6R$[a]	0.412	0.713	3.768 $c'=8c'''$	11.304 $c=24c'''$	6	$h-k+l=3n$	$2h+l=3n$	$l=3n$	$l=6n$	$R3$, $R\bar{3}$
$12R$[b]	0.410	0.711	7.536 $c'=16c'''$	22.608 $c=48c'''$	12	$-h+k+l=3n$	$h+l=3n$	$l=6n$	$l=12n$	$R32$, $R3m$, $R\bar{3}m$
$24R$[b]	0.407	0.705	15.072 $c'=32c'''$	45.216 $c=96c'''$	24	$h-k+l=3n$	$2h+l=3n$	$l=12n$	$l=24n$	$R3$, $R\bar{3}$
$2H_1$[b]	0.410	0.710	–	3.768 $c=8c'''$	2	–	–	–	$l=2n$	$P6_3$, $P6_3/m$
$2H_2$[a]	0.411	0.712	–	3.768 $c=8c'''$	2	–	$l=2n$	–	$l=2n$	$P6_3/mmc$, $P6_3mc$, $P\bar{6}2c$
$4H$[a]	0.407	0.705	–	7.536 $c=16c'''$	4	–	–	$l=2n$	$l=4n$	$P6_3/mmc$, $P6_3mc$, $P\bar{6}2c$
$12H$[a]	0.405	0.702	–	22.608 $c=48c'''$	12	–	–	$l=6n$	$l=12n$	$P6_3/mmc$, $P6_3mc$, $P\bar{6}2c$

Wu et al. [4,11,12]. $a=\sqrt{3}a'$; $c'''=0.471$ nm; $c''=1.884$ nm; c'' (height of unit layer) $=4c'''$; R: rhombohedral; H: hexagonal.
[a] New polytype.
[b] Known polytype.

positions of the unit layers ($c''=1.884$ nm) of B_2S along [$\bar{1}2\ \bar{1}0$] (Fig. 4e) were obtained using the thickness and the projective positions of the different ionic groups *d*, *e*, *f* and *g* [14,15] and the computation of the diffraction spots c'''^* (00$\underline{2}$4) and c''^* (0006) on the c^* spot array (Figs. 4a-e, 8 and 9 and Table 2).

Fig. 4f–g shows a {0001} microtwin of B_2S-6*R* to be a rotation twin with rotation angle 180°, whose twin planes and twin axes are {0001} and [0001] respectively. The diffraction spots spread in layers along the *c* direction. In the $h\bar{h}0l$ layers, two sets of diffraction spots of matrices (*M*) and twins (*T*) coincide with each other when $h=|\bar{h}|=3n$ ($n=0,\ \pm1,\ \pm2,\ldots$), but split into pairs, the split distance being 1/6 of the spot distance in the 3*n* layers (layers of the strong and stronger diffraction spots) or $c''^*/6$ when $h=|\bar{h}|\neq3n$ ($n=0,\ \pm1,\ \pm2,\ldots$). The crystal zones of the matrices (*M*) and twins (*T*) in the {0001} microtwin of B_2S (6*R*) were indexed as $[11\ \bar{2}0]_M$ and $[\bar{1}\ \bar{1}20]_T$.

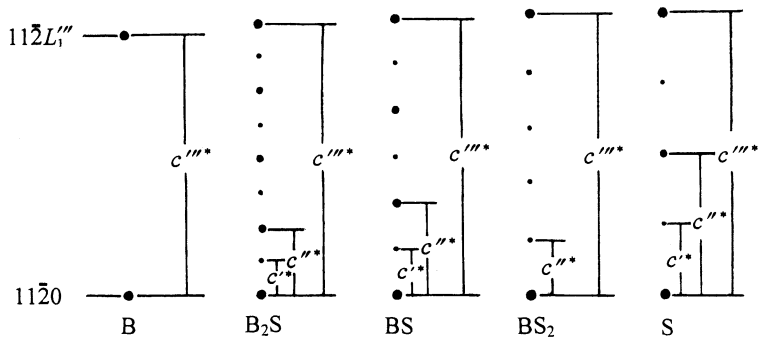

Fig. 3. Schematic representations of the $11\ \bar{2}0$–$11\ \bar{2}L_1'''$ diffraction spots in XRD rotation patterns about the *c* axis of bastnaesite (B), B_2S, parisite (BS), roentgenite (BS_2) and synchysite (S).

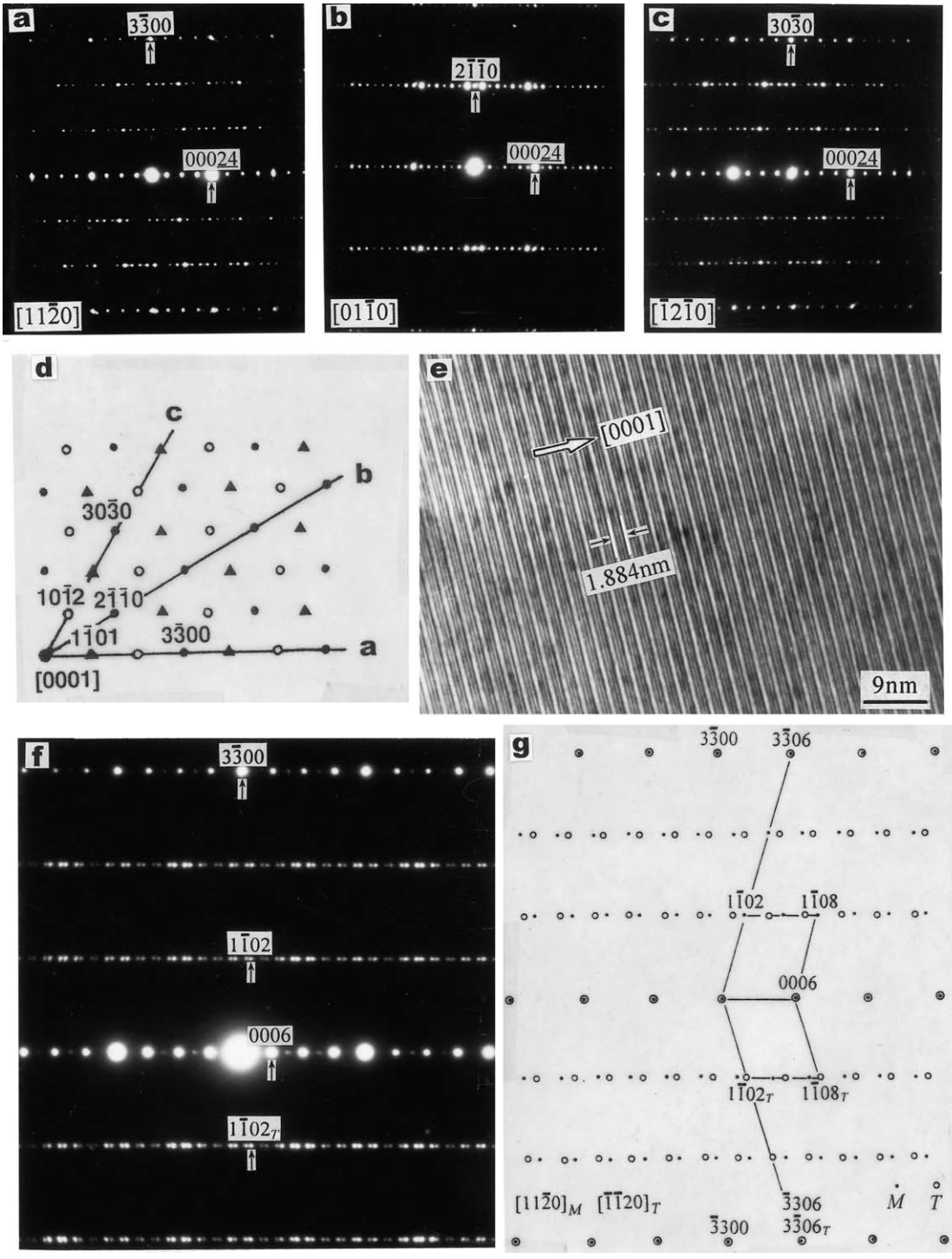
a
3̄300
00024
[11̄20]
b
2̄1̄10
00024
[01̄1̄0]
c
30̄30
00024
[1̄2̄10]
d
c
b
a
30̄30
10̄12
2̄1̄10
1̄101
3̄300
[0001]
e
[0001]
1.884nm
9nm
f
3̄300
1̄102
0006
1̄102T
g
3̄300
3̄306
1̄102
1̄108
0006
1̄102T
1̄108T
[11̄20]M [1̄1̄20]T
3̄306
3̄300
3̄306T
M
T

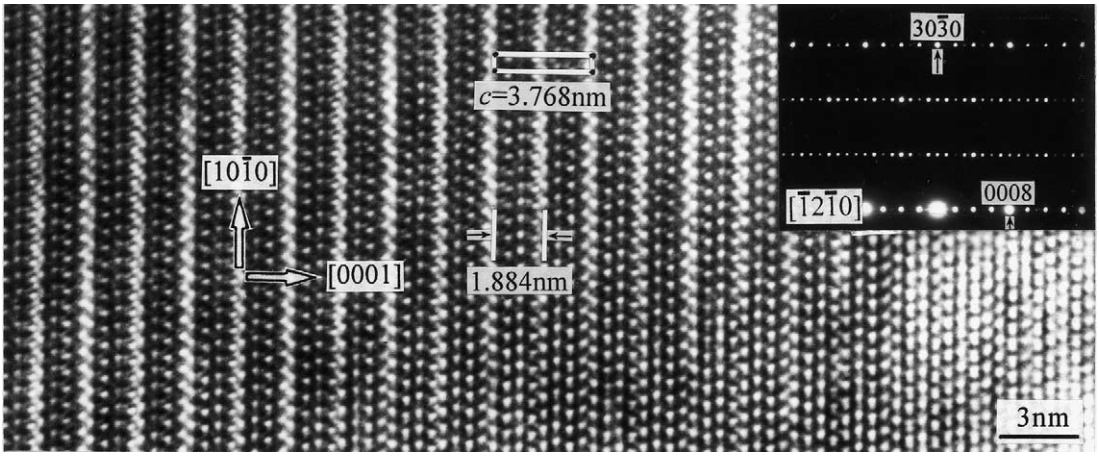

Fig. 5. SAED pattern and HRTEM image of the B_2S-$2H_1$ polytype corresponding to zones [$\bar{1}$2 $\bar{1}$0].

2.4. Three 2nH polytypes of B_2S

The polytypism of this mineral series is complex [1,8–12,16]. Four $2nH$ polytypes ($2H_1$ [11,12], $2H_2$, $4H$ and $12H$) of B_2S and three $3nR$ polytypes ($6R$, $12R$ [4,11,12] and $24R$ [11]) have been found in the 'polycrystals'. The diffraction spots in the $3n$ layers have the same arrangement in the SAED patterns of zones [$\bar{1}$2 $\bar{1}$0], [11 $\bar{2}$0] and [2 $\bar{1}$ $\bar{1}$0], revealing the same subcell dimensions $a'c'''$ and $a'c''$ ($c''=4c'''$). The distribution of the weak diffraction spots in the $3n\pm1$ layers is different and their density reveals different polytypic sequences of B_2S.

The four $2nH$ ($2H_1$ [11,12], $2H_2$, $4H$ and $12H$) polytypes of B_2S are illustrated in Figs. 5, 6 and 7a,b. Their subcells ($a'c'''$ and $a'c''$) and supercells (a c) all have hexagonal symmetry with a P lattice (Table 2 and Fig. 9). This is revealed by the distributional characteristics of the diffraction spots in the SAED patterns of zones [$\bar{1}$2 $\bar{1}$0] or [11 $\bar{2}$0] and the structural stacking mode in the HRTEM images. For example, the polytype B_2S-$2H_1$ [11,12] was recognized from the SAED and HRTEM analyses shown in Fig. 5.

Fig. 6a–d shows the SAED patterns of the crystal zones [01 $\bar{1}$0], [$\bar{1}$2 $\bar{1}$0], [$\bar{4}$5 $\bar{1}$0] and [$\bar{1}$100] in which the angles between each two adjacent zones are 29.7° (Fig. 6a,b), 19.3° (Fig. 6b,c) and 10.6° (Fig. 6c,d), respectively. In the SAED pattern of the zone [$\bar{1}$2 $\bar{1}$0], the density of the diffraction spots in the $3n\pm1$ layers and the $3n$ layers is the same, but for B_2S-$2H_1$, the density of the diffraction spots in the $3n\pm1$ layers is twice that in the $3n$ layers in Fig. 5. The spot distribution is H-lattice symmetrical (see Fig. 6a–d), so the diffraction spot nearest to the spot 0000 in the 000l spot array has the index 0002. In the case of zone [$\bar{1}$2 $\bar{1}$0] (Fig. 6e), the corresponding HRTEM image reveals an arrangement of different ionic layers and repeated periodical stacking of structural unit layers (*dededgfg*, $c''=1.884$ nm) along the c direction of the polytype B_2S-$2H_2$. Thus the cell height is made up of two unit layers (*dededgfg*), i.e. $c=2c''=2\times1.884$ nm $=3.768$ nm, and it can be called a two-layer polytype. Fig. 6f also shows an SAED pattern and HRTEM image of zone [$\bar{1}$100] of polytype B_2S-$2H_2$. Two polytypes $4H$ (a four-layer polytype) and $12H$ (a twelve-layer polytype) of B_2S are shown in Figs.

←

Fig. 4. (a–c) SAED patterns of B_2S ($6R$) obtained by tilting the crystal about [0001]. (d) A diagram of the reciprocal lattice plane determined from the SAED patterns a–c. Triangles and circles represent the spots projected onto the reciprocal lattice plane (0001)* from 1/6 $d_{(0006)}$ and 2/6 $d_{(0006)}$ above, respectively. (e) HRTEM image of B_2S ($6R$) corresponding to zone [$\bar{1}$2 $\bar{1}$0]. (f,g) SAED pattern and indexing of {0001} microtwinning in B_2S ($6R$), corresponding to zone [11 $\bar{2}$0]. Spots and circles represent the matrix (M) and twin (T).

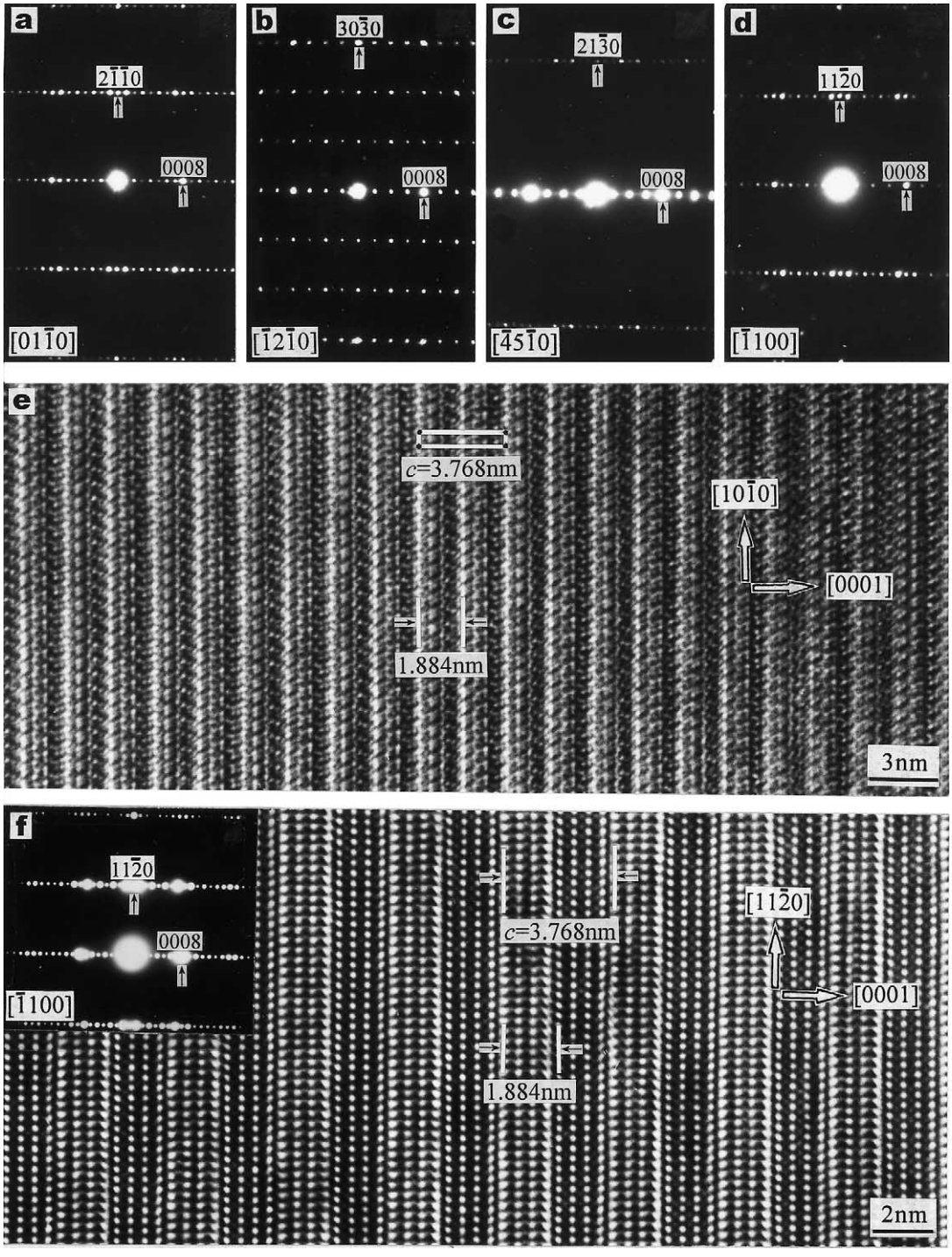

Fig. 6. (a–d) SAED patterns of the $2H_2$ polytype obtained by tilting the crystal about [0001]. (e,f) SAED patterns and HRTEM images of the B_2S-$2H_2$ polytype corresponding to zones $[\bar{1}2\ \bar{1}0]$ (e) and $[\bar{1}100]$ (f).

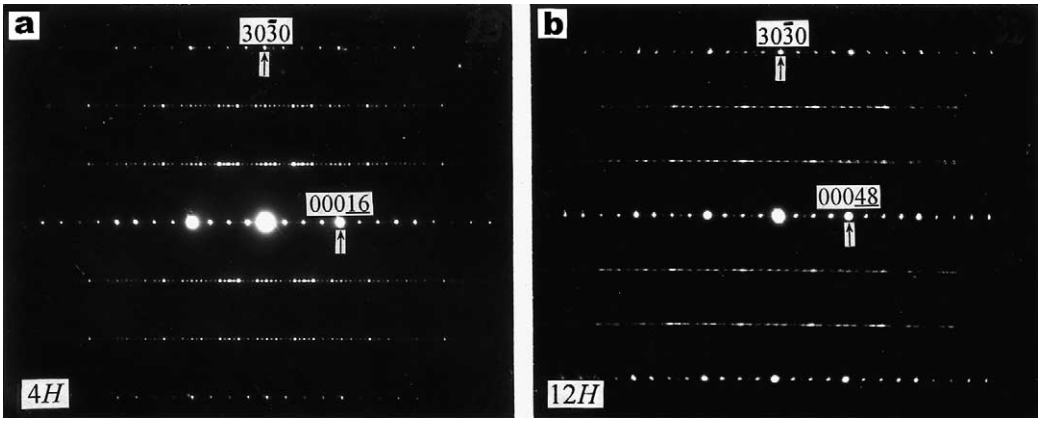

Fig. 7. SAED patterns of the B_2S-4*H* (a) and B_2S-12*H* (b) polytypes corresponding to zone [$\bar{1}2\ \bar{1}0$].

7a,b and 9 and Table 2. They have been identified by similar methods to B_2S-2H_2.

In the cases of the three 3*nR* polytypes of B_2S (6*R*, 12*R* [4,11,12] and 24*R* [11]), the smallest subcells (*a′c‴*) and subcells (*a′c″* and *a′c′*) have hexagonal symmetry, while the supercells (*ac*) are rhombohedral. In the SAED patterns of the zones [$\bar{1}2\ \bar{1}0$], [11 $\bar{2}0$] and [2 $\bar{1}\ \bar{1}0$], the reflection law of the diffraction spots is *hkil*, $-h+k+l=3n$ (12*R*) or $h-k+l=3n$ (6*R* and 24*R*) (Table 2, Figs. 4 and 9). In Fig. 4, there are five extinction spots between the transmission spot 0000 and stronger diffraction spot 0006, corresponding to a 6*R* (six-layer) polytype of B_2S.

2.5. *Syntactic intergrowths between polytypes of B_2S*

Syntactic intergrowths are a significant feature of the Ca-RE fluorocarbonate mineral series. Syntactic intergrowths among the three polytypes 2H_1, 6*R* and 4*H* of B_2S have been observed in

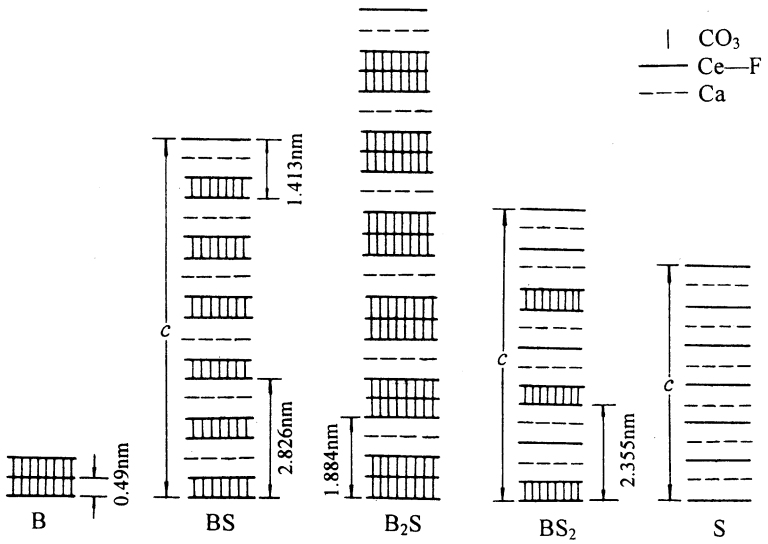

Fig. 8. Schematic representations of the crystallo-structural stacking modes of bastnaesite, the mixed-layer member B_2S, parisite, roentgenite and synchysite.

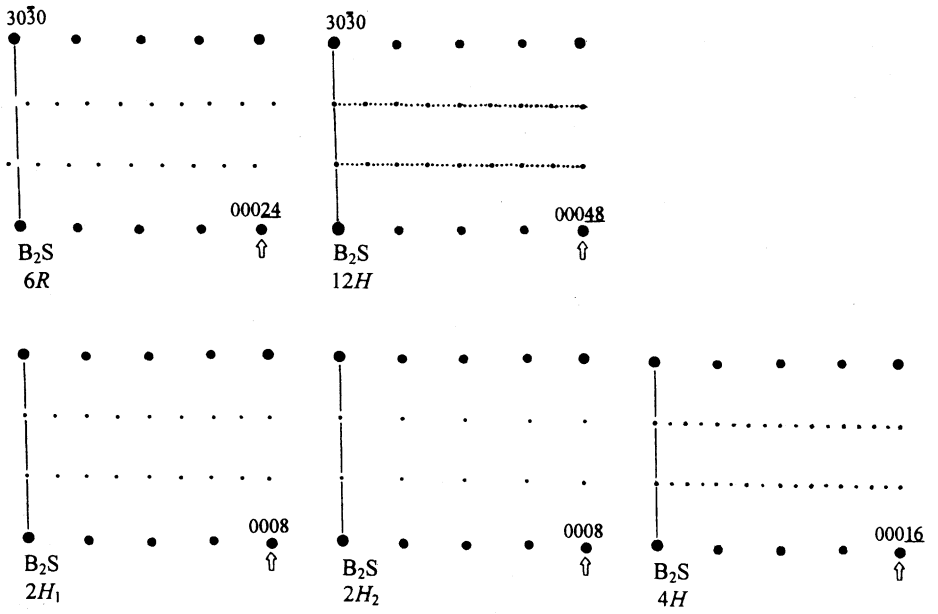

Fig. 9. Schematic representations of [$\bar{1}2\ \bar{1}0$] SAED patterns of five polytypes in B_2S.

this study. An SAED pattern of the zone [11 $\bar{2}0$] (Fig. 10b) has only one set of B_2S diffraction spots ($c'' = 1.884$ nm) along the c direction, whereas there are three sets produced by the $2H_1$, $6R$ and $4H$ polytypes superposed mutually along the $h\bar{h}0l$ spot array ($h = |\bar{h}| = 3n \pm 1$, $n = 0$, ± 1, ± 2,...). A corresponding enlarged local pattern and the results of indexing are shown in Fig. 10a, where the stronger diffraction spots nearest to the spot 0000 are produced by the lattice planes (0002) ($2H_1$), (0006) ($6R$) and (0004) ($4H$). Further research reveals that the syntactic intergrowths among different polytypes are due to a disordered stacking structure formed by the stacking faults of the unit layers along the c axis.

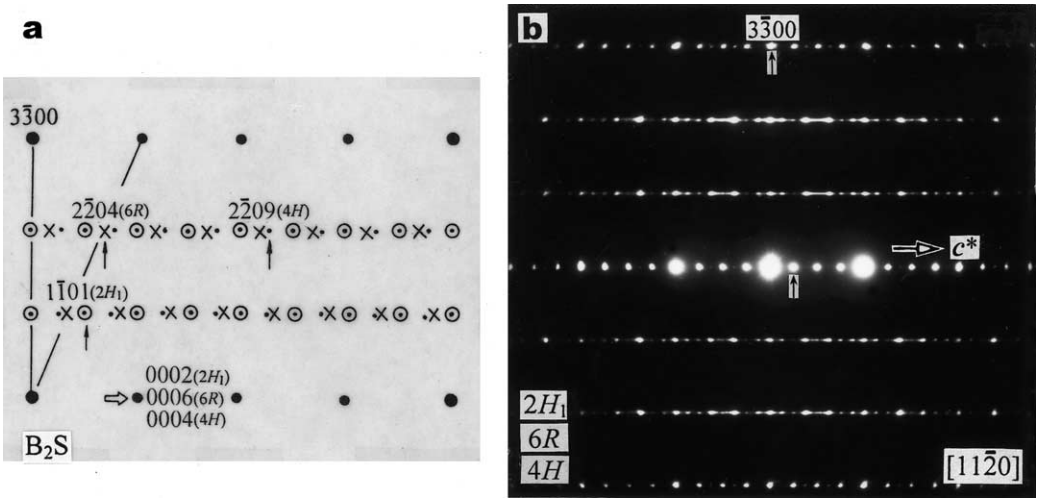

Fig. 10. (a,b) SAED pattern and indexing of syntaxic intergrowths between three polytypes in B_2S corresponding to zone [11 $\bar{2}0$].

3. Conclusions

A mixed-layer member of the Ca-RE fluorocarbonate mineral series B_2S, $CaCe_3(CO_3)_4F_3$, has been investigated by X-ray single-crystal diffraction analyses and HRTEM. Its crystal structure and chemical composition show that it is a mixed-layer member between bastnaesite-(Ce) and parisite-(Ce). Its structure (*dededgfg* or BBS) is constituted by ordered stacking of layers of bastnaesite-(Ce) (*de* or B layer) and synchysite-(Ce) (*dgfg* or S layer) in the ratio 2:1 along the *c* axis. This study reveals that B_mS_n ($m \geq n$) mixed-layer members of this series are constituted by ordered stacking of unit layers of B_2S (*dededgfg* or BBS layer) [4] and parisite-(Ce) (*dedgfg* or BS layer) [1,3,11,12,16] in different proportions along the *c* axis. For example, B_3S_2 = *dededgfgdedgfg* (or BBSBS) = *dededgfg* (or BBS) + *dedgfg* (or BS) [3,6]; B_7S_4 = *dededgfgdededgfgdededgfgdedgfg* (or BBSBBSBBSBS) = 3*dededgfg* (or 3BBS) + *dedgfg* (or BS) [7]; $B_{10}S_6$ = *dededgfgdededgfgdededgfgdedgfgdedgfgdedgfg* (or BBSBBSBBSBBSBSBS) = 4*dededgfg* (or 4BBS) + 2*dedgfg* (or 2BS) [7];.... An accurate knowledge of the crystal structure and superstructure of B_2S is therefore essential to characterize minerals of this goup.

Four new polytypes ($2H_2$, $4H$, $12H$ and $6R$) with a grain size greater than 0.5 μm have been discovered in the 'polycrystals' of this mineral series. All except $2H_2$ have long-period stacking structures with c = 7.536–22.608 nm, and always occur as polycrystals with disordered stacking sequences and microtwins along with other mixed-layer members and other mineral species of the series. The subcell heights of these polytypes are identical, whereas their supercell heights are different. The latter reveal the variations of the stacking period and arrangement of the unit layers *dededgfg* in the long-period stacking sequences. These new polytypes are mainly formed by periodic variations of the relative displacements of the CO_3 groups between the structural layers *dededgfg* in the B_2S.

The {0001} microtwin of B_2S-$6R$ has been observed and identified by HRTEM. Syntactic intergrowths among the three polytypes $2H_1$, $6R$ and $4H$ have also been discovered, revealing variations of stacking disorder of the structural layers *dededgfg* and aperiodicity in the orientation arrangement of CO_3 groups between the layers. This provides important microscopic information about the growth environment and mechanism of formation of this mineral series.

Acknowledgements

This project was supported by the National Natural Science Foundation of China (Grants Nos. 40172019, 49872069 and 49102019), the Natural Science Foundation of Hubei Province, China (2001ABB004), the Foundation for Key University Teachers of the Ministry of Education of China (GG-709-10491-1008), and the Laboratory for Quantitative Prediction and Exploration Assessment of Mineral Resources and the National Land Resources Ministry of China. Thanks also go to two referees for their thoughtful comments and constructive suggestions that helped improve the original manuscript.*[AC]*

References

[1] G. Donnay, J.D.H. Donnay, The crystallography of bastnaesute-(Ce), parisite-(Ce), roentgenite-(Ce) and synchysite-(Ce), Am. Mineral. 38 (1953) 932–963.
[2] G. Donnay, Roentgenite-(Ce), a new mineral from Greenland, Am. Mineral. 38 (1953) 868–870.
[3] J. Van Landuyt, S. Amelinckx, Multiple beam direct lattice imaging of new mixed-layer compound of the bastnaesite-synchysite series, Am. Mineral. 60 (1975) 315–318.
[4] X.L. Wu, G.M. Yang, Z.L. Pan, X.H. Wang, Lattice image study of new mixed-layer minerals in calcium rare-earth fluorocarbonate mineral series (in Chinese), Acta Mineral. Sin. 11 (1991) 193–199.
[5] G.M. Yang, Z.L. Pan, X.L. Wu, Transmission electron microscopic study of new regular stacking structure in calcium rare-earth fluorocarbonate mineral series from Southwest China (in Chinese), Sci. Geol. Sin. 29 (1994) 393–398.
[6] X.L. Wu, D.W. Meng, J. Liang, Z.L. Pan, Ordered-disordered stacking structure along the *c*-axis in calcium rare-earth fluorocarbonate minerals, Proceedings 30th International Geological Congress, VSP International Science Publishers, The Netherlands, Vol. 16, 1997, pp. 49–57.
[7] X.L. Wu, D.W. Meng, Z.L. Pan, Transmission electron microscopic study of new, regular mixed-layer structures

in calcium-rare-earth fluorocarbonate minerals, Mineral. Mag. 62 (1998) 55–64.
[8] Y.X. Ni, J.E. Post, J.M. Hughes, The crystal structure of parisite-(Ce), Ce_2CaF_2 $(CO_3)_3$, Am. Mineral. 85 (2000) 251–258.
[9] D.W. Meng, X.L. Wu, T. Mou, D.X. Li, Determination of six new polytypes in parisite-(Ce) by means of high resolution electron microscopy, Mineral. Mag. 65 (2001) 797–806.
[10] D.W. Meng, X.L. Wu, T. Mou, D.X. Li, Microstructural investigation of new polytypes in parisite-(Ce) by high-resolution electron microscopy, Can. Mineral. 39 (2001) 1713–1724.
[11] X.L. Wu, G.M. Yang, Z.L. Pan, Discovery of B_mS_n polytypes and study of microstructure in calcium-rare-earth fluorocarbonate minerals (in Chinese), J. Chin. Electron Microsc. Soc. 11 (1992) 216–221.
[12] X.L. Wu, G.M. Yang, Z.L. Pan, A TEM study of syntaxies formed from the polytypes of parisite(BS) and regular mixed-layer mineral B_2S (in Chinese), Acta Mineral. Sin. 13 (1993) 214–219.
[13] X.H. Wang, Study on crystal structure and crystal chemistry of calcium rare earth fluorocarbonate mineral series of Maoniuping, Sichuan, and its preliminary systematic mineralogy, Thesis for the Doctorate, China University of Geosciences, 1991, pp. 62–66 (in Chinese).
[14] Y.X. Ni, J.M. Hughes, A.N. Mariano, The atomic arrangement of bastnaesite-(Ce), $Ce(CO_3)F$, and structural elements of synchysite-(Ce), roentgenite-(Ce), and parisite-(Ce), Am. Mineral. 78 (1993) 415–418.
[15] L.B. Wang, Y.X. Ni, J.M. Hughes, P. Bayliss, J.W. Drexler, The atomic arrangement of synchysite-(Ce), $CeCaF(CO_3)_2$, Can. Mineral. 32 (1994) 865–871.
[16] Z.M. Yang, K.J. Tao, P.S. Zhang, The symmetry transformation of modules in bastnaesite-vaterite polysomatic series, Neues Jahrbuch für Mineralogie Monatshefte, 1998, pp. 1–12.